Characterisation and Modelling of Meshed Electrodes on Free Standing Polyvilylidene Difluoride (PVDF) Films for Enhanced Pyroelectric Energy Harvesting

Zabek*, D., Taylor, J., and Bowen, C. R.
University of Bath, Bath, BA2 7AY, UK
*e: D.Zabek@bath.ac.uk

Abstract: Flexible pyroelectric energy generators provide unique features for harvesting temperature fluctuations which can be effectively enhanced using meshed electrodes that improve thermal conduction, convection and radiation into the pyroelectric. In this paper, thermal radiation energy is continuously harvested with pyroelectric free standing Polyvilylidene Difluoride (PVDF) films over large numbers of heat cycles using a novel micro-sized symmetrical patterned meshed electrode. It is shown that, for the meshed electrode geometries considered in this work, the polarisation-field (P-E), current-field (I-E) characteristics and device capacitance are unaffected since the fringing fields were generally small; this is verified using numerical simulations and comparison with experimental measurements. The use of meshed electrodes has been shown to significantly improve both the open circuit voltage (16V to 59V) and closed-circuit current (9nA to 32nA). The pyroelectric alternating current (AC) is rectified for direct current (DC) storage and a 30% reduction in capacitor charging time is achieved by using the optimum meshed electrodes. The use of meshed electrodes on ferroelectric materials provides an innovative route to improve their performance in applications such as wearable devices, novel flexible sensors and large scale pyroelectric energy harvesters.

Keywords: Pyroelectric energy harvesting, PVDF, meshed-, patterned electrodes.

1. Introduction

The harvesting of waste energy from industrial, transportation and domestic applications continues to attract attention. Common forms of ambient energy include mechanical vibrations as well as natural or externally induced temperature oscillations and these sources

can be converted into electrical energy using solid-state generators utilising the piezo- and pyro-electric effect. Ferroelectric materials are of interest for such applications since they exhibit both piezo- and pyro-electric behaviour and can be used in generator mode for both thermal and vibration energy harvesting devices [1]. For thermal harvesting applications the ferroelectric material experiences thermal fluctuations, which results in a change in the level of polarisation ΔP [C/m^2] (permanent orientation polarisation). On a macroscopic level this change in polarisation interacts at the material electrode interfaces which accumulate positive or negative surface bound charges on the surface of the ferroelectric. When the polarisation changes, this free bound charge is effectively the product of the change in temperature ΔT [K] and change in polarisation ΔP. For a pyroelectric material with a thermal charge coefficient (pyroelectric coefficient) p^* [C/m^2 K] the electric field E [V/m] generated at open circuit conditions is given by [2]:

$$E = \frac{\Delta P}{\varepsilon_r . \varepsilon_0} = p^* . \Delta T \tag{1}$$

where ε_r is the relative permittivity of the material and the permittivity of free space is ε_0 [F/m]. The electric field generated is the potential difference (V) divided by the thickness (h) is then defined by the material geometry ($E=V/h$). Under short circuit conditions, the instantaneous pyroelectric current I [A] is:

$$I = p^* . A . \frac{dT}{dt} \tag{2}$$

for a pyroelectric with an electrode surface area A [m^2]. When the conductive electrodes that are applied to the polarised surfaces of the ferroelectric fully cover the perpendicular materials polarisation plane, the electric field can be assumed to be static with the potential difference homogeneously distributed across the electrode surface area, since many natural temperature fluctuations driving pyroelectric energy harvesting applications operate at relatively low frequencies. The capacitance of this type of energy harvesting system can be approximated by the parallel plate capacitor theory, which provides a linear definition of the systems electrical capacitance C [F]:

$$C = \varepsilon_r . \varepsilon_0 \frac{A}{h} \tag{3}$$

for a given dielectric thickness h [m]. To account for the transformed energy Q [J] stored in the capacitive element, the energy equation [3]:

$$Q = \frac{1}{2} C . V^2 \tag{4}$$

provides the available electrical charge energy.

1.1 Meshed Electrodes for Pyroelectric Energy Harvesting

According to equation 4, the energy trade off from a fixed geometry energy harvesting systems can be improved by maximising the potential difference in equation (1), assuming a constant capacitance. For pyroelectric applications, the use of symmetrical meshed electrodes [4] or non-symmetrical woven electrodes [5] has the potential to improve any thermal conduction, [6], convection and radiation [7] into the ferroelectric and therefore can enhance the available change in temperature ΔT, or rate of change in temperature ($\Delta T/\Delta t$). When subjected to thermal radiation, a fully covered metallic electrode acts to reflect the energy. However, if partially covered meshed electrodes are employed, the pyroelectric materials are directly exposed to the heat source due to the presence of openings in the reflective electrode so that the pyroelectric active material largely absorbs thermal radiation around the 700 nm wavelength [8], removing energy from the radiation beam with increasing penetration depth.

Meshed-, interdigiated- or woven- partially covered electrodes can be manufactured by a controlled deposition or by a selective removal of the electrode area while maintaining the initial geometry of the energy harvesting system. Figure 1 shows a schematic of a pyroelectric material (Polyvilylidene Difluoride- PVDF) and the meshed electrode structure examined in this work. This is illustrated by a decreasing amplitudes of the irradiation arrows in Figure 1. Consequently, the pyroelectric active materials with a meshed electrodes have the potential to achieve higher absolute changes in temperatures (and therefore higher open circuit voltages) and faster- and higher-rates of change in temperature (and therefore higher closed circuit currents).

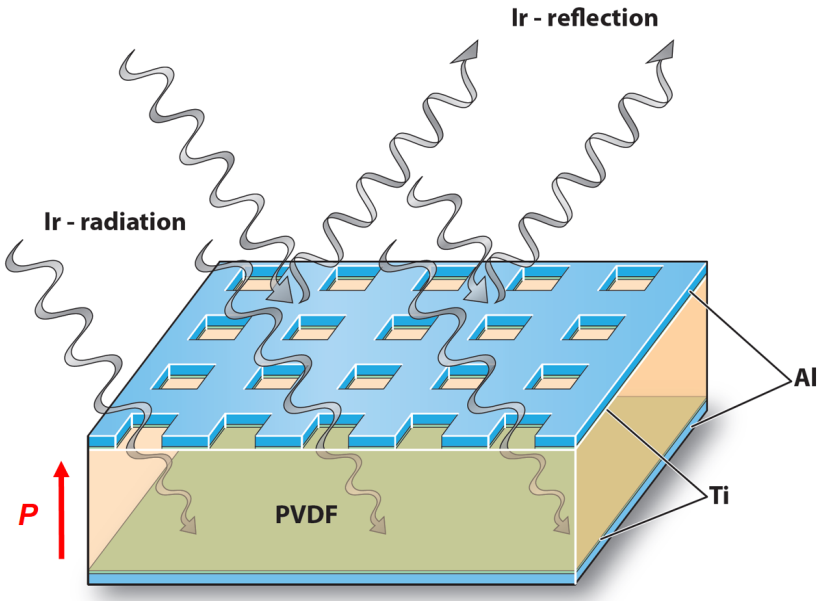

Figure 1: Pyroelectric harvester with meshed electrodes exposed to thermal radiation. In this work the Ti interlayer is 4nm, Al layer is 200 nm, PVDF is 52 µm thick and electrode windows are 10 x10 µm.

For tested meshed structures in this work, symmetric temperature oscillations were introduced in order to harvest pyroelectric energy by switching a Philips 175 W infra-red (IR) lamp (PAR38) 'on' for heating at 293 mW/cm^2 (measured using a calibrated thermal power sensor THORlabs – Germany) and 'off' for convective cooling at constant room temperature (22 °C). Since the test devices were exposed to the radiation only at the upper electrode absorbance and transmittance, neglecting back-reflections, for the aluminium electrode [9] and pyroelectric active PVDF [10] are shown in Figure 2 for comparison. For the un-electroded PVDF film, the wavelength dependent radiation absorption coefficient decays from a nearly perfect absorption of 0.97 at shorter wavelengths to 0.2 at longer wavelengths at the far end of the visible light spectrum. The radiation absorption of PVDF significantly improves across all wavelengths with thicker PVDF films in the range of 320 μ m [10]. The aluminium absorption coefficient remains low at just below 0.2 for all wavelengths in Figure 2.

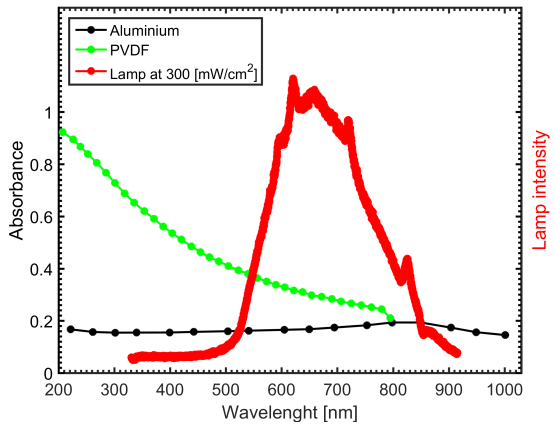

Figure 2: Radiation absorbance and lamp emittance with wavelength for Aluminium and PVDF.

According to equation 3 and 4, the electrode area of a parallel plate capacitor with meshed electrodes for pyroelectric energy harvesting is defined as the total surface area (A) of the material perpendicular ($\perp$) to the average ferroelectric polarisation (P) moment (Figure 1) subtracted by the open mesh surface area (in this case the square windows) that is directly exposed to the IR radiation beam:

$$\textit{Electrode coverage} = A_{\perp, P} - A_{\perp, P} \textit{ exposed to IR radiation} \quad (5)$$

The fully electroded surface area of the PVDF film therefore represents 100 % coverage as a reference, This definition applies for the experimental results reported as well as for the modelling conducted in this paper.

This work introduces meshed electrodes for pyroelectric energy harvesting followed by a detailed characterisation of materials and harvesting structures formed using micro-size symmetrical square meshed electrodes. The polarisation-electric field (P-E) behaviour, piezoelectric displacement (strain-electric field), and pyroelectric polarisation with a series of different electrodes covering between 19 % and 100 % of the ferroelectric material surface are studied followed by a coupled field finite element analysis (FEA) for the electrostatic capacitance. Since the electrodes proposed do not fully cover the ferroelectric material they do not satisfy the homogeneity assumption with two parallel plates from equation (3). The electrodes meshed geometry leads to the formation of complex electric fields patterns followed by irregular charge concentrations at the edges, fringing electrical fields and 'dead' zones across the dielectric [11]. Consequently, the effective permittivity (capacitance), piezo- and pyro-electric non-linearities can affect the energy conversion of the solid-state generator with a potential decrease in electrical storage capabilities [12]. The modified electrode geometry is simulated in the FEA model and the complex electric field distribution is studied.

For this work the meshed electrode devices are formed on low permittivity and low stiffness β-phase Polyvilylidene Difluoride (PVDF); this material is of particular interest due to its molecular purity, consistent properties and high electric fields strength. Other attractive properties are that compared to ferroelectric ceramics, such as lead zirconate titanate (PZT) or high performance single crystals such as lead magnesium niobate - lead titanate (PMN-PT), the use of PVDF and PVDF-copolymers (PVDF-TrFE or PVDF-TrFE-CFE) provide high flexibility, low density, good bio-compatibility, scalability, transparency, and low cost. These properties have attracted the attention of these materials for portable or wearable ultra-low power electronic devices for health care monitoring [13], intermittent wireless communication, and autonomous power supplies reducing the need for batteries and primary energy fuels.

2. Experimental set-up for pyroelectric energy harvesting and polarisation

2.1 Electrode structure and formation of meshed electrode

To form the meshed electrodes, squares (or ‘windows’) are selectively removed from a fully covered aluminium electrode using a low cost wet etching process, precise details are given in [4], The materials are then poled with the meshed electrode structure. The ferroelectric

polymer was an extruded 52 μm PVDF film (Precision Acoustics, UK) with an electrode with a titanium (2 nm) – aluminium (200 nm) electrode on both sides using a sequential electron beam vapour deposition system (Edwards FL-400). The 2 nm bonding layer of titanium was introduced to prevent pinhole generation, oxide formation, strip breaks, nano-cracks and improve adhesion and durability with the polymer films [14]. This was followed by a lithographic direct laser writing process in order to expose a (10 x 10) μm^2 square pattern array and wet etch the metal electrode windows, the device was poled. Figure 3 shows and example of the device structure which is the side view of the actual manufactured meshed electrode on PVDF; in this case the electrode has a 75 % electrode area coverage (defined by equation 5) with 'windows' 10 μm by 10 μm in size. The decrease in the electrode surface area coverage is achieved by a gradual increase in the number of removed (10 x 10) [μm^2] squares n per unit area by the factor n^2; this is undertaken in order to obtain a symmetrical meshed top electrode geometry.

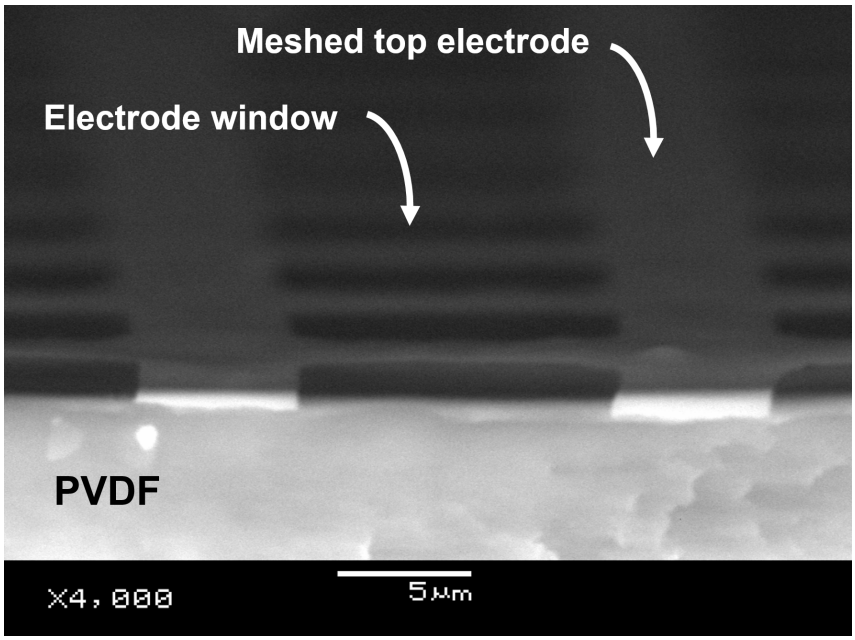

Figure 3: Scanning electron micrograph (SEM) of side view of upper section of a PVDF-meshed electrode harvester with 75 % electrode surface area coverage. The polarisation direction of the PVDF is through thickness. The lower electrode (not shown in this image) is continuous.

2.2 Characterisation of harvesting devices

2.2.1 Polarisation, strain - electric field, and capacitance with meshed electrodes on PVDF

When employing meshed electrodes there is a potential to form a non-uniform electric field distribution throughout the device. This is experimentally verified by measurement of the ferroelectric hysteresis loops (P-E loops) and capacitance to characterise the average macroscopic polarisation, this includes the non-electroded areas of the mesh in Figures 1 and 3. Using a Sawyer-Tower circuit, a 1Hz and 10kV triangle wave was cycled from positive to negative in order to record the remnant polarisation using an aixACT (Germany) PES test system with the sample immersed in Dow Corning (US) silicone fluid during the test. The applied electric field - polarisation was measured for 25, 43, 76, 91 % meshed- and fully covered 100 % reference electrodes on previously reported PVDF films until dielectric breakdown at around 2 MV/cm occurred [4]. For pyroelectric systems, which require a change in temperature in order to develop a potential difference, the temperature dependence of the material properties as well as the high electric field hysteresis loops with PVDF were studied by heating the test chamber to 50 ºC [15]. Piezoelectric strain – electric field was measured for a 52 μm thick PVDF film on a fully covered electrode geometry using an aixDBLI double beam laser interferometer at the centre of the sample. Electrical impedance spectroscopy (EIS) measurements (Solatron S1 1260 impedance analyser) for the 25 % to 100 % electroded PVDF films were examined to determine the change in device capacitance with electrode coverage.

2.2.2 Open circuit voltage and closed circuit current

For pyroelectric electrical characterisation, the meshed PVDF films were exposed to the cycled infra-red (IR) light beam operating at a frequency of 0.05 Hz in order to establish harmonic temperature oscillations with constant average temperatures. For cyclic heating, the transient open circuit voltage and closed circuit was recorded using a Keithley (US) 6514 electrometer with an input impedance of 100 TΩ and a sensitivity of 10 pA.

2.2.3 Rectification and storage of pyroelectric energy

While it is of interest to characterise the improvements in open circuit voltage and short circuit current, in practical energy harvesting applications there is a need to store the harvested energy or subject the energy harvester to an electrical load. Since temperature oscillations are usually small and slow, the non-ideal pyroelecric alternating supply current (AC) is variant in time and magnitude and for this reason some form of power conditioning is needed. In addition, most silicon based electronics require a direct current (DC) power supply requiring rectification when harvesting thermal energy with pyroelectric.

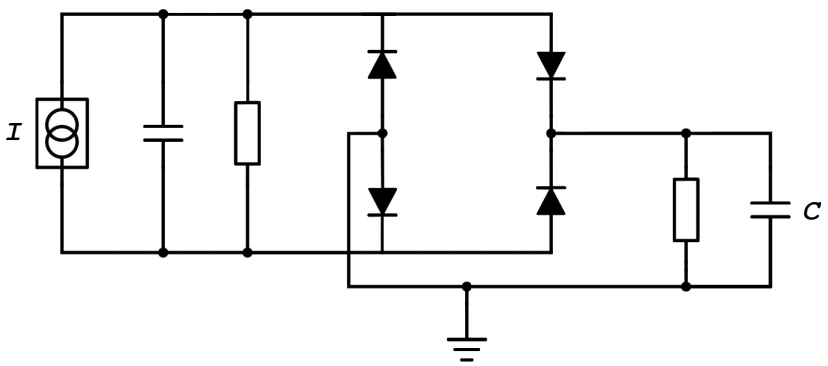

Figure 4: Full wave bridge rectifier circuit used to supply an external storage capacitor during thermal cycling.

Therefore, in this work the electrical energy as a result of irradiation of the material with an IR lamp is transformed into a symmetrical full wave bridged rectifier circuit that was formed from four diodes (Vishay GP02) and the energy was harvested by free standing pyroelectric PVDF film with an area of (10 x 10) [mm^2] with a 52 μm thickness. The cycled IR beam current from the pyroelectric generator (I) was then rectified and discharged into an external capacitance output (C). The corresponding electric circuit diagram in Figure 4 shows the standard h-bridge configuration employed supplying the rectified electrical energy into an external storage 100 nF (AVX) multilayer ceramic capacitor (C). According to the energy harvesting circuit in Figure 4, various meshed pyroelectric PVDF samples were exposed to the cycled IR beam while the rectified capacitor terminal voltage was recorded. The terminal DC voltage for the storage capacitor was measured using a Keithley 6514 electrometer.

2.3. Finite element analysis of meshed electrodes using coupled field model

The charge-voltage relationship and piezoelectric displacement with applied electric field are numerically evaluated and compared with experimental results for PVDF films in order to resolve polarisation, electric field distribution and capacitance with meshed electrodes and non-homogeneous electric fields. The specific capacitance of a (100 x 100) [μm^2] and 52 μm thick element is modelled as a close approximation for the meshed electrodes of area (10 x 10) [mm^2] and 52 μm thick free standing PVDF films and shows the electric field patterns at the electrode corners, the edges, and the areas between the equally spaced squares in the 3-dimensional (3-D) space in Figure 1 [16]. With the electrodes modelled as two dimensional layers, the PVDF is considered unclamped. Following the piezoelectric constitutive equations for the mechanical stress T_{ij} [N m^{-2}] and the displacement D_i [m] [17]:

$$\begin{Bmatrix} T_{ij} \\ D_i \end{Bmatrix} = \begin{bmatrix} c_{ijkl}^E & -e_{kij} \\ e_{ikl} & \varepsilon_{ij}^{ST} \end{bmatrix} \begin{Bmatrix} S_{kl} \\ E_k \end{Bmatrix}$$

the stiffness matrix c_{ijkl} [Pa] under constant electric field E, permittivity ε_{ij} under constant stress S [N/m^2] and temperature T [°C], and piezoelectric charge coefficient e_{ikj} [C m^{-2}] (constant stress), was solved with the commercially available FEA package ANSYS 15. With the PVDF film poled through the thickness (3- or z- direction), the anisotropic mechanical and electrical bulk properties for uniaxial mechanically stretched PVDF films provided by the manufacturer [18] are compared against the literature for the piezoelectric charge coefficient [17]:

$$e_{ij} = \begin{bmatrix} & & & & & 0.18533 \\ & & & & & 0.08869 \\ & & & & & -0.41678 \\ & & & & & \\ & & & -0.49091 & & \\ -0.33333 & & & & & \end{bmatrix}$$

and the elastic compliance [19]:

$$c_{ij}^E = 10^{-10} \begin{bmatrix} 3.61 & 1.61 & 1.42 & & & \\ & 3.13 & 1.31 & & & \\ & & 1.63 & & & \\ & & & 0.55 & & \\ & & & & 0.55 & \\ & & & & & 0.69 \end{bmatrix}$$

and the relative permittivity at constant stress [20]:

$$\varepsilon_o^{ST} = \begin{bmatrix} 11 & & \\ & 11 & \\ & & 11 \end{bmatrix}$$

which applies to most piezo-electric and pyroelectric systems that are free to deform (unclamped) [21]. When the piezoelectric system is clamped, constant stress permittivity for the crystallographic 3-3 direction is converted into constant strain permittivity employing the electromechanical coupling coefficient k [-] [3]:

$$k_{33} = \frac{d_{33}}{\sqrt{s_{33}\varepsilon_{33}}} \tag{5}$$

satisfying most piezoelectric load conditions.

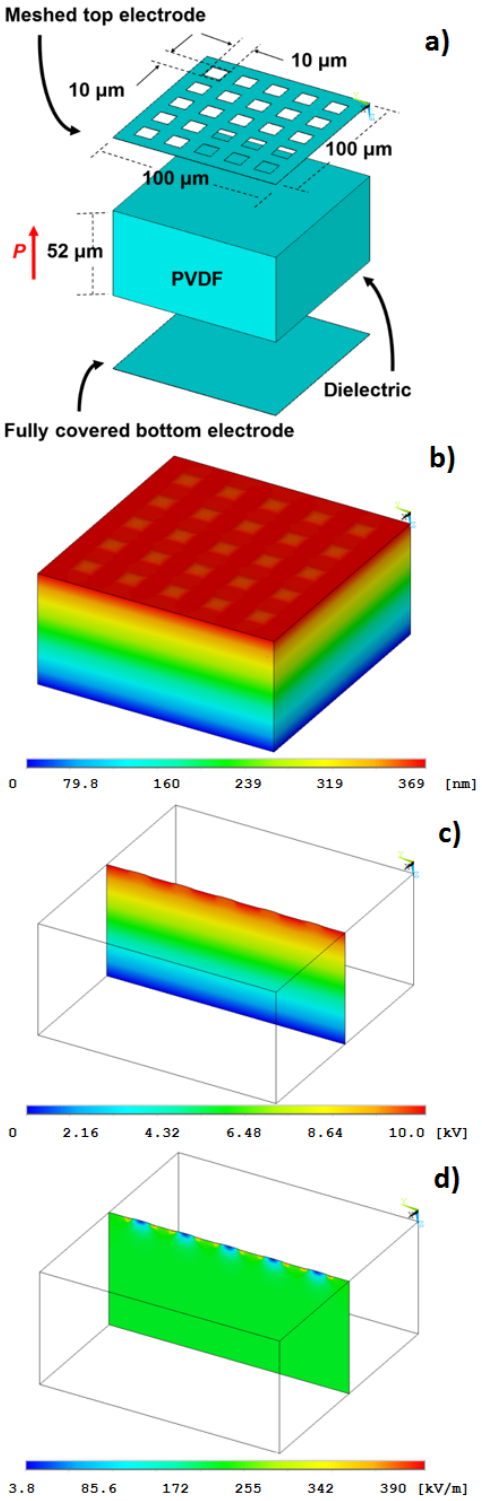

Figure 5: Finite element model of meshed electrodes showing geometry (a), piezoelectric displacement (b) electric-potential through thickness (c) and electric field through thickness (d) with 75 % coverage.

The coupled field analysis of the PVDF film in Figure 5 (a) enables the analysis of the local electric field distribution around the meshed electrodes and the local piezoelectric

displacement in Figure 5 (b) for the local electric field. For the electric equipotential in Figure 5 (c) the numerical solution of the inhomogeneous distribution around the top electrode shows a small fringing electrical flux in Figure 5 (d); this will be described in more detail in the result section and the influence or electrode area coverage and the aspect ratio, defined as the ratio of PVDF thickness to window dimension, on model outputs.

3. Results and discussion

3.1 Hysteresis loops of meshed electrodes

For energy harvesting it is important to understand the dominant source capacitance and peak voltage of the pyroelectric element with meshed electrodes in order to account for the transformed energy; for example equation 3 which is the parallel plate assumption and the source capacitance in Figure 4. For this reason, the electrostatic macroscopic polarisation was measured. Figure 5 (a) and (b) shows a coarse series of meshed electrodes. According to equation 5, the coarse series of PVDF – Al/Ti meshed electrodes was manufactured with an electrode surface coverage of 25, 43, 76, 91 and a fully covered 100 % references electrode for comparison. The electrode coverage for the constant surface area was gradually decreased maintaining the meshed square feature size of 10 μm starting with 91 % down to 25 %. While the specific level of polarisation (*P*) is calculated by the available charge density over the total area (10 x 10 mm^2), the electric field remains electrode geometry independent ($E = \sigma/\varepsilon$). Constant values for remnant polarisation (P_r = 6 μC cm^2) and coercive field (E_c = 750 kV cm) with decreasing surface coverage were observed up to electric fields of 1950 kV/cm; at higher field electrical breakdown was observed (Figure 6 a).

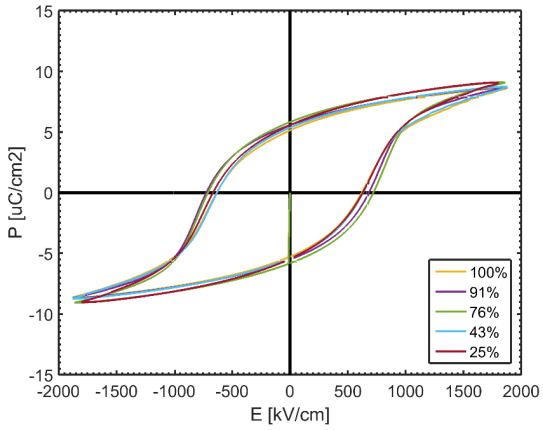

(a)

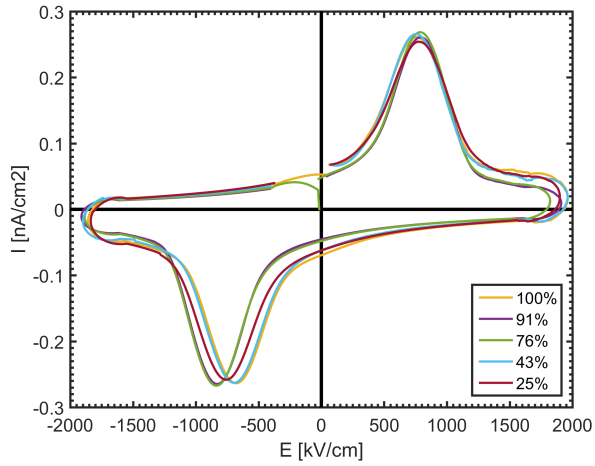

(b)

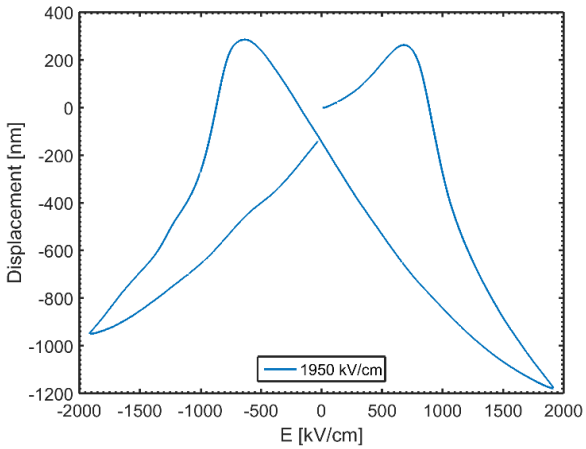

(c)

Figure 6: Ferroelectric polarisation – applied electric field (P-E) loop of PVDF with various meshed electrode areas. (b) current – applied electric field (I-E) loop for various meshed electroded (c) and piezoelectric displacement of PVDF with fully covered electrode for externally applied electric field.

In the corresponding current-field (I–E) loop, see Figure 6 b, a current peak is produced as a result of ferroelectric domain motion at the coercive field. This also shows a constant current magnitude for a decreasing electrode surface coverage which leads to a constant energy consumption of the capacitive element with meshed electrodes (equation 3). Therefore, the average polarisation - surface electrode interaction of the fully covered bottom electrode and the coarse series of the partially covered top electrode structure from Figure 1 does not change with a decreasing electrode surface coverage. The driving current for the greatly reduced electrode surface coverage of reduced 25, 43, 76 and 91 % does not change, for which reason an identical equivalent 100 % reference capacitance is observed, these

observations are compared later in the paper where device capacitance is compared with the finite element simulations. Figure 6 c shows the strain-field response with applied electric field. Data for the fully covered electrode are only shown since the meshing electrode has an influence on the infereometer signal. The contraction of the film is the sum of the piezoelectric effect and the electrostrictive effect working in favour of the piezoelectric displacement primarily due to the low permittivity and highly elastic properties of PVDF and the negative piezoelectric e_{33} coefficient of -0.416 C m^2, allowing the PVDF film to contract when an external field is applied [22]. The maximum displacement magnitude is ~1150 nm at an applied voltage 10 kV across the 52 μm PVDF film in Figure 5. The modelled displacement in the FEA model at this large electric field is ~367 nm for an identical external voltage since it neglects electrostrictive effects and enhanced strain due to domain orientation at such high electric fields.

3.2 Temperature dependent polarisation

When recovering electrical energy from heat, the temperature changes developed and the change in dipole moment due to pyroelectric effects, the permittivity and the nonlinear dielectric behaviour are of interest [23]. Under moderate thermal conditions below 80 °C, PVDF is of particular interest for pyroelectric energy harvesting application due to the low permittivity and high thermal conductivity followed by a high volumetric energy density when manufactured in thin films and large areas [24]. For the fully covered (100%) reference electrode, Figure 7 shows the P-E loop for PVDF between room temperature (25 °C) and 50 °C and compares the change in properties for this particular temperature range where changes in ambient temperature are likely. The coercive filed decreases slightly (from 750 kV/cm to 700 kV/cm) with an increase in temperature, as does the remnant polarisation. According to equation 2, the calculated change in polarisation P for a performed change in temperature **Δ**T of 25 °C with PVDF is 82 nC for a 1 cm^2 PVDF film ($p^* = 25$ μC m^2 K^{-1} [25]). Under elevated temperatures the coercive field decreases because the molecular mobility increases with temperature improving ferroelectric switching.

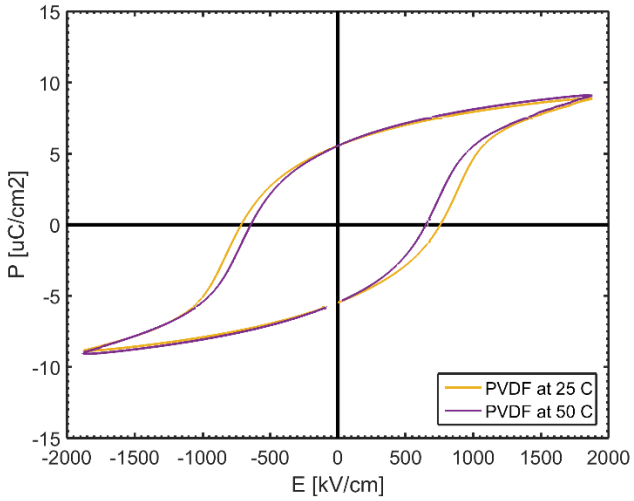

Figure 7: Ferroelectric polarisation – applied electric field (P-E) loop at 1 Hz for PVDF with fully covered electrode at room temperature and 50°C.

3.3. Capacitance and electrical field distribution

The energy density of the energy harvesting systems, and therefore the electrical capacitance, needs to be assessed in order to assess the performance of different generators (Equation 4). The small changes in P-E and I-E loops with increasing meshed area in Figure 6 indicate that a constant energy storage capability with meshed electrodes despite a decreasing electrode coverage. In this section we will compare the measured capacitance of meshed electrodes with numerical simulations.

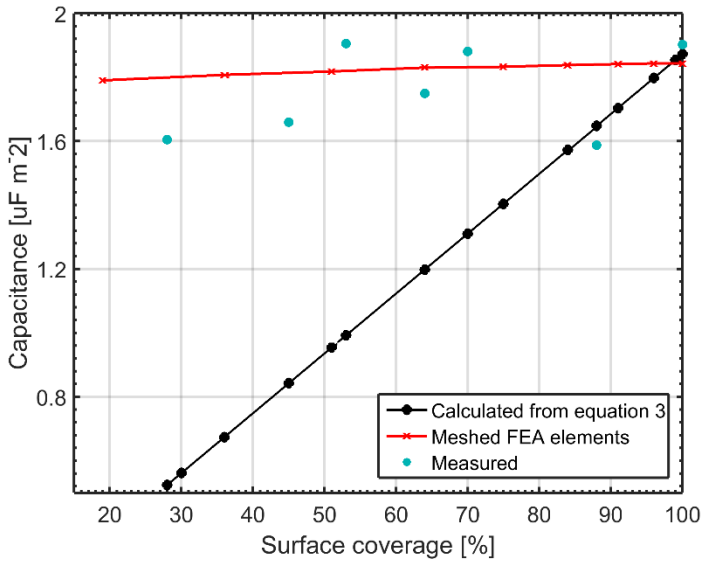

Figure 8: Variation of device capacitance with electrode surface coverage. The measured values are compared with the FEA prediction and parallel plate assumption.

According to the parallel plate assumption in equation 3, the electrical capacitance is calculated assuming a parallel electrical flux (ignoring fringing fields) with respect to the meshed upper electrode area (*A*). For this reason, Equation 3 predicts a linear decrease in capacitance with a decrease in electrode coverage. With the FEA model taking into account the fringing fields, dielectric and piezoelectric displacement for the applied electric field, Figure 8 compares the calculated (equation 3) with FEA capacitance together with the experimental measurements for 25, 43, 76, 91 and 100 % electrode area samples. For the 100% area coverage all three approaches (measured, numerical and parallel plate) are in good agreement. However, the experimental and numerical finite element results show a slow decrease in capacitance with decreasing electrode surface coverage. Compared to the fully covered electrode, with a 18 $\mu F/m^2$ reference capacitance, the 19 % covered electrode geometry shows only a 4 % lower capacitance for the numerical simulation of 17.28 $\mu F/m^2$ in Figure 8 [16]. The experimental results show an extrapolated reduction in capacitance of 8 %. This leads to the conclusion that the average electric field strength remains constant for the device geometry examined in this work, despite a non-homogeneous parallel plate geometry.

3.4.1 Electric field distribution

The origin of the relatively constant device capacitance and polarisation-field loops with meshed electrode area can be explored via the numerical modelling where the meshed top electrode structure maintains the same level of charge as the fully covered bottom electrode followed by local charge concentrations and high electrical fields.

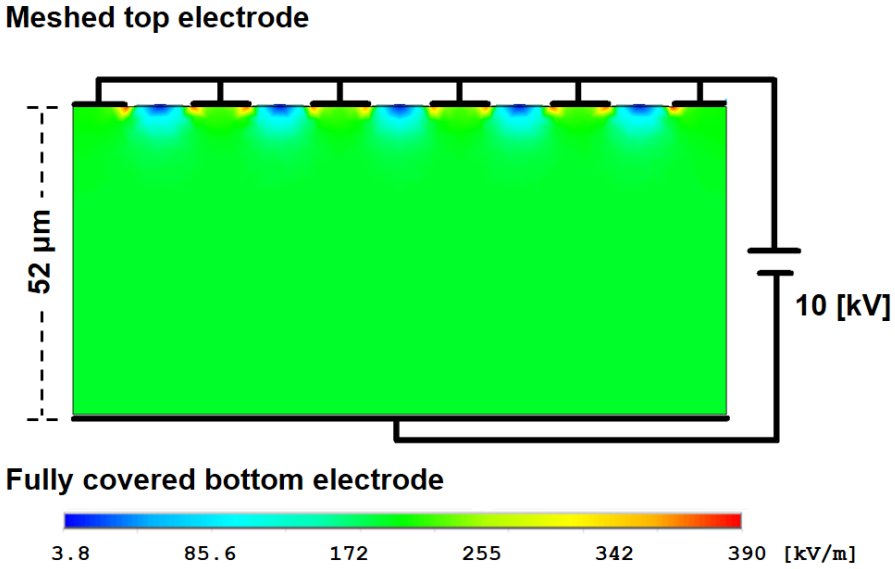

Figure 9: 2-D plane showing the electric field distribution through the PVDF thickness for a meshed electrodes (in the case, electrode coverage area is 75%).

Based on the FEA model for the electric flux within the ferroelectric, Figure 9 provides the local electric field distribution of the 2 dimensional (2-D) plane from the Figure 5 (d) model. The non-linear electric field lines in Figure 8 developed around the electroded areas of the meshed top electrode are fringing towards the fully covered bottom electrode. In contrast, the electric field strength decreases around the non-electroded areas of the meshed top electrode. Consequently, the piezoelectric displacement weakens for a lower strength electric field creating slight bumps at the surface of the PVDF film due to a lack of piezoelectric strain (see upper surface in Figure 5b). High electric fields dominate the meshes top electrode with a peak electric field strength 2.2 greater than the average field. Towards the fully covered bottom electrode, the electric field becomes parallel at approximately $1/10^{th}$ of the dielectric thickness of 52 µm where the low 3.8 kV/m field vanishes. Where electric field lines are parallel, the parallel plate assumption and therefore the capacitance from equation 3 is justified. This condition is determined by the dielectric thickness h and the spacing between the conductors of the meshed electrode [16]. In this model, the aspect ratio of the dielectric thickness 52 µm to the mesh spacing of 10 µm between in the conductors relates to a 5.2, for which the parallel plate assumption for non-homogeneous electrodes is a sufficiently accurate assumption.

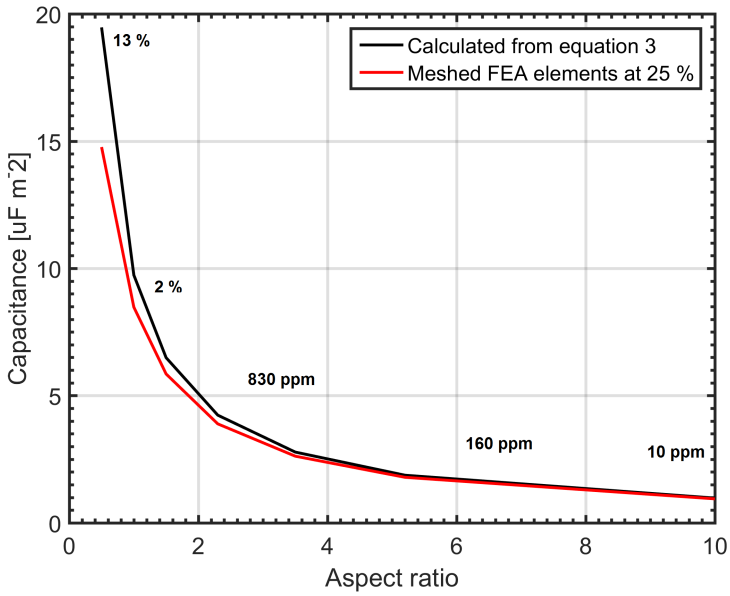

Figure 10: Influence of PVDF thickness to window dimension aspect ratio on the device capacitance. The numbers indicate the % difference between the parallel plate assumption and the finite element simulations.

With high aspect ratios above five, where the ferroelectric is much thicker than the electrode spacing, the parallel plate assumption provides a good approximation of the systems geometry with parallel electric fields. However, for thin dielectrics with a large electrode spacing (low aspect ratio), most electric field lines are fringing and the available capacitance decreases. Figure 10 shows the discrepancy between calculated capacitance assuming a homogeneous electric flux and the modelled capacitance of a meshed electrode 10 μm spacing for varying aspect ratios. For an aspect ratio of 0.5, with a dielectric thickness of 5 μm and a spacing of ~10μm, the modelled capacitance of 15 μF m^2 is 25 % lower than the ideal calculated capacitance of 20 μF m^2 (equation 3). For larger aspect ratios, e.g. greater than four, the fringing electrical fields quickly recover the electrical storage capabilities of the meshed energy harvesting system.

3.5 Open circuit voltage and short-circuit current

When characterising pyroelectric materials, the generated closed circuit current and the open circuit voltage with the corresponding change in temperature and rate of change in temperature as a result of incident thermal radiation provides an indication of device performance. According to the experimental test conditions reported in section 1.1, the pyroelectric response with meshed electrodes is experimentally analysed. Assuming identical thermal boundary conditions for all electrode surface coverages, for a gradual decrease in electrode surface coverage from a fully covered 100 % reference electrode to a 45 % covered meshed top electrode, there is an observed increase in in ΔT in Figure 11 (a). This greater change in temperature is followed by an increase in open circuit voltage (Figure 11 c) and closed circuit current (Figure 11 d). The cycled open circuit peak voltage in Figure 11 c improves from 16 V to at 100 % coverage to 59 V at 45 % electrode coverage for constant irradiance as does the closed circuit peak current in Figure 11 d from 9 nA to 32 nA, respectively [4].

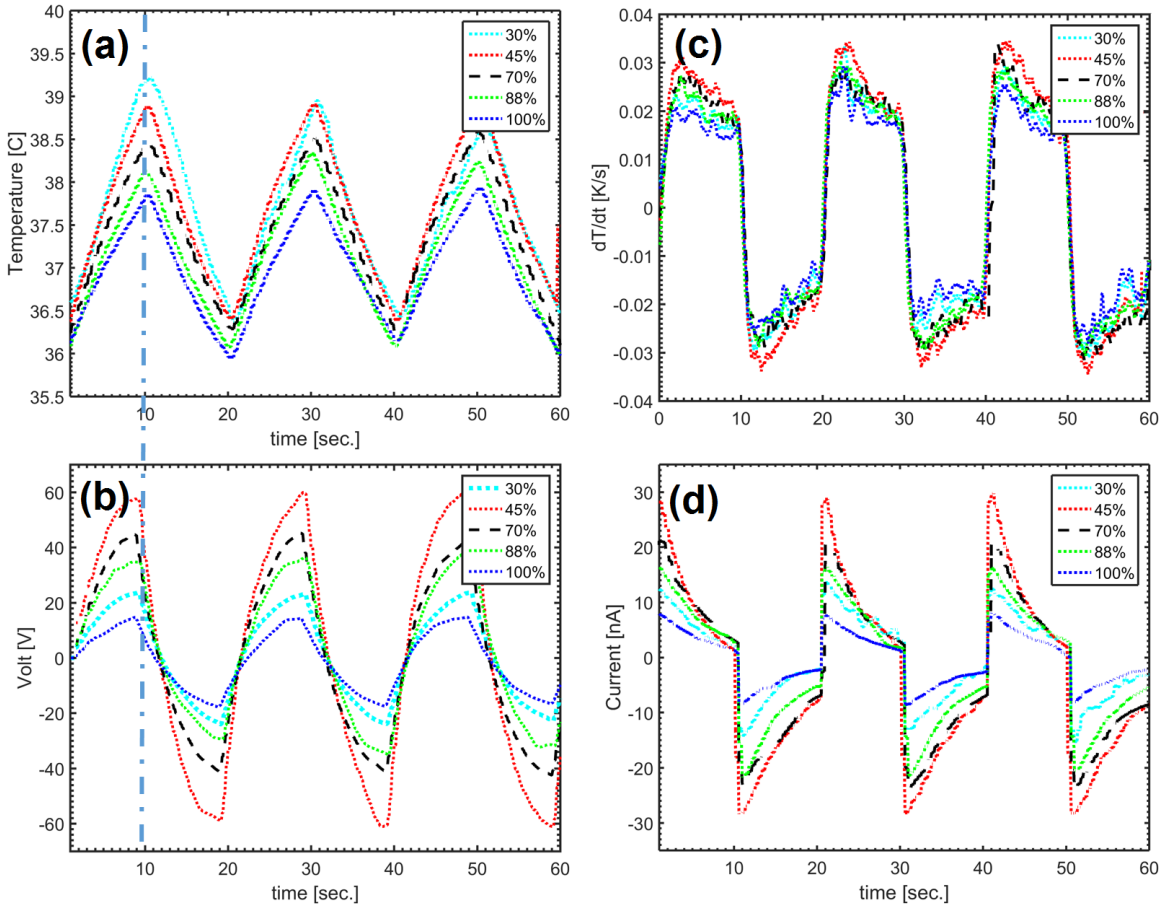

Figure 11: Energy transformation performance with meshed electrodes and decreasing electrode surface coverage (modified from [4]*).*

The pyroelectric peak performance at 45 % with meshed electrodes was reported for an identical geometry with corona poled meshed samples [4] and is confirmed for electrode poled samples, showing a rapid performance decrease when the electrode coverage is being removed greatly.

3.6 Rectification and storage

While improvements in open circuit voltage and short circuit current are of interest, in practical energy harvesting applications there is a need to store the harvested energy. When optimising an energy harvesting systems and the device performance, small and slow thermal oscillations are challenging. Unlike impedance matching with high resistive external loads for PVDF [26], more sophisticated Synchronised Switching Harvesting (SSH) improves the systems energy conversion can further improve the systems energy conversion [22].

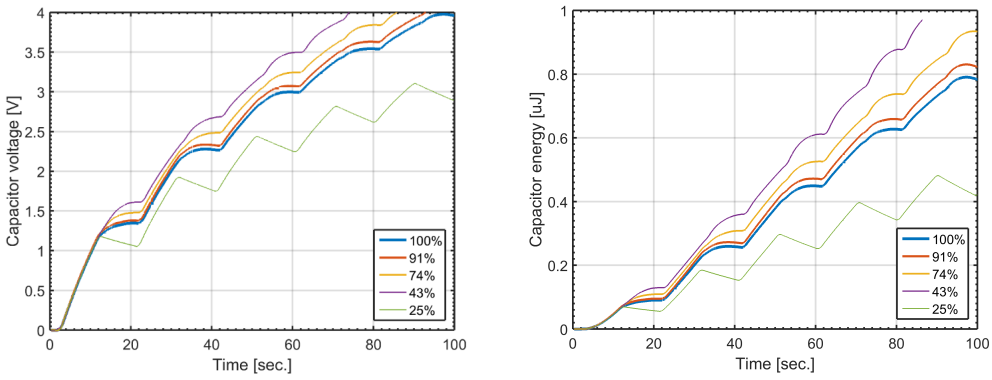

(a) (b)

Figure 12 (a) capacitor voltage and (b) harvested thermal energy with meshed electrodes stored in an external 100 nF capacitance.

Figure 12 compares the charging performance with the rectifier circuit from Figure 3 of the fully covered 100 % reference electrode with meshed 91, 74, 43 and 25 % covered samples external capacitance over five thermal cycles. The rectified instantaneous current from Figure 10 d is stored in the external capacitive element as a potential difference accumulating the harvested electrical energy. The capacitor voltage of 4 V after 100 second of continuous charging shows a steady increase for the fully covered reference electrode in Figure 4. With meshed electrodes, the 4 V potential difference was reached after 84s with the 74 % covered meshed electrode and after 70s with the 43 % covered meshed electrode, respectively. Compared to the fully covered electrode, the 43 % covered meshed electrode charges the rectification circuit 1.42 times faster, improving device performance, efficiency and energy conversion. Further improvements is charging time can be achieved for higher capacitor voltages. However, when reducing the electrode coverage to 25 %, the meshed PVDFs film is unable to build up the external capacitor voltage to 4 V within 100 seconds, underperforming the fully covered design. According to equation 4, the energy stored at the external 100 nF capacitor at 4 volt corresponds to 0.8 µJ. Figure 12 compares the energy for the individual PVDF samples for continuous thermal cycling. The benefit with meshed electrodes is the quicker charge build up enabling faster thermal cycles harvesting more energy. Due to the squared dependency of the stored energy (equation 4), meshed electrode significantly improve pyroelectric energy harvesting.

Conclusions

The intrinsic electro-mechanical and thermal properties of PVDF have a great potential for piezoelectric and pyroelectric energy harvesting systems. It has been demonstrated that for

pyroelectric systems, meshed electrodes provide a novel approach to improve energy conversion of a PVDF energy harvester. For the meshed electrodes considered in this work the polarisation-field (P-E) and current-field (I-E) characteristics are unaffected since the use of small micro-sized windows leads to fringing fields which maintain a relatively homogenous electric field. The effects of poling are studied and the meshed electrode structure fully characterised. The capacitance remains quasi-linear with a decrease of up to 4 % with respect to decease in electrode surface coverage and this is in good agreement with numerical predictions of device capacitance. For the electrical energy stored in the meshed electrode - dielectric system, high electric fields and complex distributions are present. It has been shown for electrode geometries where the aspect ratio of thickness to window dimension of greater than five, the parallel plate assumption is shown to be a good approximation for a constant geometry dielectric materials. It has been shown that the available capacitance and the potential energy conversion characteristics falls for only large electrode windows and thin films, i.e. meshed systems with low aspect ratio. The use of meshed electrodes has been shown to significantly improve both the open circuit voltage (16V to 59V) and closed-circuit current (9nA to 32nA); which has implication for both energy harvesting and sensor applications. Due to the nature for heat thermal energy harvesting and waste heat recovery, slow and small temperature oscillations require conditioning circuits. In the simplest form, the full wave bridge rectifier harvests thermal energy. With a 45 % meshed electrode, the charging time was reduced by 30% compared to a fully covered architecture. The use of a partially covered electrode on ferroelectrics, such as PVDF thin films, provides scope to widen the range of potential energy harvesting applications due to the beneficial material properties of flexibility, toughness and ease of fabrication as free-standing films for applications such as wearable devices, novel flexible sensors, nano-scale devices and large scale pyroelectric energy harvesters.

Acknowledgements

The research leading to these results has received funding from the European Research Council under the European Union's Seventh Framework Programme (FP/2007-2013) / ERC Grant Agreement no. 320963 on Novel Energy Materials, Engineering Science and Integrated Systems.

Reference

[1] Bowen, C. R., Kim, H. A., Weaver, P. M., & Dunn, S. (2014). Piezoelectric and ferroelectric materials and structures for energy harvesting applications. Energy & Environmental Science, 7(1), 25-44. doi:10.1039/C3EE42454E

[2] Lang, S. B. (1974). Sourcebook of pyroelectricity (Vol. 2): CRC Press.

[3] Moulson, A., & Herbert, J. (1990). Electroceramics Chapman and Hall. New York, 41.

[4] Zabek, D., Taylor, J., Boulbar, E. L., & Bowen, C. R. (2015). Micropatterning of Flexible and Free Standing Polyvinylidene Difluoride (PVDF) Films for Enhanced Pyroelectric Energy Transformation. Advanced Energy Materials, 5(8), n/a-n/a. doi:10.1002/aenm.201401891

[5] Zhu, R., Chung, C.-H., Cha, K. C., Yang, W., Zheng, Y. B., Zhou, H., Li, G. (2011). Fused silver nanowires with metal oxide nanoparticles and organic polymers for highly transparent conductors. ACS nano, 5(12), 9877-9882.

[6] Kim, M.-S., Jo, S.-E., Ahn, H.-R., & Kim, Y.-J. (2015). Modeling of a honeycomb-shaped pyroelectric energy harvester for human body heat harvesting. Smart Materials and Structures, 24(6), 065032.

[7] Hsiao, C.-C., Ciou, J.-C., Siao, A.-S., & Lee, C.-Y. (2011). Temperature field analysis for PZT pyroelectric cells for thermal energy harvesting. Sensors, 11(11), 10458-10473.

[8] Hammes, P., & Regtien, P. (1992). An integrated infrared sensor using the pyroelectric polymer PVDF. Sensors and Actuators A: Physical, 32(1), 396-402.

[9] Bartl, J. and Baranek, M., 2004. Emissivity of aluminium and its importance for radiometric measurement. Measurement of Physical Quantities, 4(3), pp.31-36.

[10] Solvay; 2015.Technical Data Sheet. http://solvay.com/

[11] Vendik, O. G., Zubko, S. P., & Nikol'skii, M. A. (1999). Modeling and calculation of the capacitance of a planar capacitor containing a ferroelectric thin film. Technical Physics, 44(4), 349-355. doi:10.1134/1.1259300

[12] Chiu, Y., Lee, M., & Wu, S. (2015). PDMS-based flexible energy harvester with Parylene electret and copper mesh electrodes. Journal of Micromechanics and Microengineering, 25(10), 104007

[13] Dagdeviren, C., Yang, B. D., Su, Y., Tran, P. L., Joe, P., Anderson, E., Feng, X. (2014). Conformal piezoelectric energy harvesting and storage from motions of the heart, lung, and diaphragm. Proceedings of the National Academy of Sciences, 111(5), 1927-1932.

[14] Keles, O., & Dundar, M. (2007). Aluminum foil: Its typical quality problems and their causes. Journal of Materials Processing Technology, 186(1), 125-137.

[15] Kubouchi, Y., Kometani, Y., Yagi, T., Masuda, T., & Nakajima, A. (1989). Structure and dielectric properties of vinylidene fluoride copolymers. Pure and applied chemistry, 61(1), 83-90

[16] Zabek, D., Bowen, C., & Taylor, J. (2015). Electrical capacitance with meshed electrodes for piezo-and pyro-electric energy harvesting applications. Paper presented at the Applications of Ferroelectric, International Symposium on Integrated Functionalities and Piezoelectric Force Microscopy Workshop (ISAF/ISIF/PFM), 2015 Joint IEEE International Symposium on the.

[17] Sokhanvar, S., Dargahi, J., Najarian, S., & Arbatani, S. (2012). Piezoelectric Polymers: PVDF Fundamentals Tactile Sensing and Displays (pp. 37-65): John Wiley & Sons, Ltd.

[18] PVDF Properties and Uses, Precision-Acoustics-Ltd., Dorset 2013, http://acoustics.co.uk/wp-content/uploads/2013/12/Properties-ofpoled-PVDF.pdf (accessed April 2014).

[19] Varadan, V. V., Roh, Y. R., Varadan, V. K., & Tancrell, R. H. (1989, 3-6 Oct 1989). Measurement of all the elastic and dielectric constants of poled PVDF films. Paper presented at the Ultrasonics Symposium, 1989. Proceedings., IEEE 1989.

[20] Gregio, R, and Ueno, E. M., Effects of crystalline phase, orientation and temperature on the dielectric properties of poly(vinylidene dluoride) (PVDF). Journal of Material Science, 34(18), 4489-4500. Doi: 10.1023/a:1004689205706

[21] Lanceros-Mendez, S., Moreira, M. V., Mano, J. F., Schmidt, V. H., & Bohannan, G. (2002). Dielectric Behavior in an Oriented β-PVDF Film and Chain Reorientation Upon Transverse Mechanical Deformation. Ferroelectrics, 273(1), 15-20. doi:10.1080/001501902117

[22] Zhao, X.-Z., Bharti, V., Zhang, Q., Romotowski, T., Tito, F., & Ting, R. (1998). Electromechanical properties of electrostrictive poly (vinylidene fluoride–trifluoroethylene) copolymer. Applied physics letters, 73(14), 2054-2056.

[23] Guyomar, D., Sebald, G., Lefeuvre, E., & Khodayari, A. (2008). Toward heat energy harvesting using pyroelectric material. Journal of intelligent material systems and structures.

[24] Bowen, C., Taylor, J., Le Boulbar, E., Zabek, D., & Topolov, V. Y. (2015). A modified figure of merit for pyroelectric energy harvesting. Materials Letters, 138, 243-246.

[25] Bowen, C., Taylor, J., LeBoulbar, E., Zabek, D., Chauhan, A., & Vaish, R. (2014). Pyroelectric materials and devices for energy harvesting applications. Energy & Environmental Science, 7(12), 3836-3856.

[26] Belhora, F., Cottinet, P.-J., Guyomar, D., Petit, L., Lebrun, L., Hajjaji, A., .Boughaleb, Y. (2013). Optimization of energy harvesting conversion using the hybridization of electrostrictive polymers and electrets. Sensors and Actuators A: Physical, 189, 390-398.